

# Grazing-incidence Mössbauer spectroscopy determination of photo- and conversion-electron yield functions

M. A. Andreeva, S. M. Irkaev, and V. G. Semenov

Moscow State University, 119899 Moscow, Russia

(Submitted 28 January 1994)

Zh. Eksp. Teor. Fiz. **105**, 1767–1784 (June 1994)

Simultaneous quantitative analysis of a series of Mössbauer mirror-reflection and secondary-electron yield spectra was performed. The spectra were obtained for different grazing angles from an oxidized 50-nm thick  $^{57}\text{Fe}$  film. The analysis is based on the general theory of propagation of resonant radiation in an inhomogeneous layered medium under conditions of total reflection. Stepped profiles of the electron density and photoelectric absorption and the depth profile of resonance nuclei with different hyperfine interactions were obtained. The photo- and conversion-electron yield functions were also determined and were found to be different nonmonotonic functions of the depth.

## 1. INTRODUCTION

In x-ray and Mössbauer optics the secondary radiation, which is directly affected by variations of the radiation field in the medium, can be used effectively in order to study the crystalline and magnetic structure of solids. Investigations of secondary processes are most informative under the conditions of Bragg diffraction (the method of standing x-ray waves<sup>1,2</sup>) or grazing-incidence diffraction<sup>3</sup> and in combination with spectral investigations (Mössbauer or EXAFS spectroscopy<sup>4,5</sup>).

Due to their shallow emergence depths ( $\sim 10$ – $300$  nm) photo- or conversion electrons yield structural information about ultrathin layers near the surface. The depth selectivity in this case is determined by the so-called yield function  $T(z)$ , which determines the probability that a secondary electron knocked out at depth  $z$  will reach the detector. Finding the yield function for electrons in different energy groups is a nontrivial and very important problem, both from the standpoint of checking the theory of electron propagation in matter and for correct interpretation of the experimental results obtained by recording photo- or conversion electrons.

Yield functions can be calculated theoretically only for ideal samples whose composition is uniform and whose properties do not vary with depth.<sup>6,7</sup> In practice, however, even ideal crystals, to say nothing about finely dispersed films, are structurally imperfect in an ultrathin surface layer, and many experimental investigations are conducted without energy analysis or with quite rough energy resolution. In addition, the parameters of the counter and the geometry of the experiment strongly affect the experimental results.

There are very few empirical determinations of the yield function. Such investigations can be performed under conditions of dynamic Bragg diffraction<sup>8–9</sup> or total external reflection<sup>10–12</sup> of x-ray radiation, when the penetration depth of the radiation in the medium varies in a prescribed manner over a range comparable to the depth at which

photoelectrons appear. In Ref. 12 investigations were carried out of the angular dependence of the yield of photoelectrons in different energy groups near the critical angle of total reflection of 14.4 keV x-rays from an iron film and the yield functions were determined from these data. Based on the belief that the photo- and conversion-electron yield functions with excitation by radiation with the same wavelength are identical, the intention was to employ the results for the interpretation of the Mössbauer conversion spectra.

In the present work we have made the first simultaneous determination of the yield functions for photo- and conversion electrons by the method of grazing-incidence Mössbauer spectroscopy.<sup>13</sup> Our approach to solving this problem is based on a new effect which we recently discovered: the resonant behavior for the detected photoelectrons under conditions of total external reflection of the Mössbauer radiation.<sup>14</sup> In contrast to Ref. 12, we analyzed not the angular dependence of the secondary-radiation yield but rather the shape of the Mössbauer spectrum near the critical angle of total reflection. Under these conditions the spectral shape depends on the relative contribution of both photo- and conversion electrons emerging from different depths to the recorded spectrum. This is what makes it possible to determine their yield functions separately.

## 2. GENERAL THEORY FOR THE EMERGENCE OF SECONDARY RADIATION

The probability distribution  $P^s$  for the production of secondary particles by the transmitted radiation is determined, in the general case, in an absorbing gyrotropic medium by the expression<sup>15</sup>

$$P^s = w^s / 2(\mathbf{E} * \hat{\sigma} \mathbf{E}), \quad (1)$$

where  $w^s$  is the probability for the production of a particle of type  $s$  per absorption event,  $\mathbf{E}$  is the amplitude of the electric field of the radiation, and  $\hat{\sigma}$  is the conductivity tensor, defined as the antihermitian part of the generalized

susceptibility tensor  $\hat{\chi}$  of the medium. For a monochromatic plane wave with frequency  $\omega$  we can write

$$\hat{\sigma} = \frac{\omega}{4\pi i} \frac{\hat{\chi} - \hat{\chi}^+}{2}. \quad (2)$$

In the case when the Mössbauer radiation propagates in a resonant medium the radiation is absorbed both in atomic electron shells and by resonant nuclei. For this reason the susceptibility  $\hat{\chi}$  and, correspondingly, the conductivity  $\hat{\sigma}$  consist of two parts

$$\hat{\chi}(\omega) = \hat{\chi}^{\text{nuc}}(\omega) + \chi^{\text{el}}, \quad (3)$$

where the nuclear part of the susceptibility  $\hat{\chi}^{\text{nuc}}$  is characterized by a strong dependence on the small shifts in the energy of the incident radiation in the resonance region  $\hat{\chi}^{\text{nuc}} = \hat{\chi}^{\text{nuc}}(\omega)$ . For our experimental arrangement it is significant that the nuclear and electronic parts of the susceptibility of the medium ( $\lambda = 0.086$  nm) are very small:  $|\chi| \sim 10^{-5}$ .

The interaction with the electronic subsystem is usually of a scalar character, and the expression (2) for this part of the conductivity simplifies while the expression (1) for the case of photoelectron production becomes

$$P^{\text{el}} = \frac{\omega}{8\pi} \omega^s \text{Im } \chi^{\text{el}} |\mathbf{E}|^2, \quad (4)$$

where  $\text{Im } \chi^{\text{el}} = \lambda/2\pi\mu$  and  $\mu$  is the linear photoelectric absorption coefficient. The probability distribution  $P^{\text{nuc}}$  of secondary-radiation production under nuclear resonance conditions can also be represented similarly when it can be assumed that the resonant interaction is isotropic.

Secondary radiation produced at different depths  $z$  arrives and is recorded by a detector with different probability, called the secondary-radiation yield function  $T(z)$ :

$$I^s(\omega) = \int_0^\infty P^s(z, \omega) T(z) dz, \quad (5)$$

where  $I^s(\omega)$  is the resonance spectrum of the yield of secondary radiation. In order to compare with the experimental Mössbauer spectrum  $I^s(\omega)$  of the secondary-radiation yield it is necessary to form the convolution with the line-shape of the resonant source.

Electron propagation in matter is accompanied by losses and "spreading" of the initial electron energy. Electrons are emitted with no energy loss practically only from the surface. When electrons are detected at a fixed energy, the maximum of the electron yield function  $T(z)$  is displaced into the interior of the medium and is broadened, the broadening being larger the more this energy differs from the initial energy of the knocked-out electron. When the emerging electrons are integrated over energy the yield function is usually represented as either an exponential or a quadratic polynomial, whose coefficients are calculated taking into account random collisions by the Monte Carlo method.<sup>6,7</sup> They depend on the initial energy of the electrons, the atomic number of the particles, the electron density in the medium, and so on. In any case, however, the average depths from which the conversion or Auger electrons can emerge from the sample is significantly smaller

than the penetration depth of x-rays; this is what determines the surface sensitivity of Mössbauer conversion spectroscopy.

First we consider qualitatively how the two contributions (photo- and conversion electrons) are manifested in the measured secondary-electron yield spectrum in different cases. In order to simplify the discussion we assume that the medium is semi-infinite and uniform and that the yield functions  $T^{\text{el}}(z)$  and  $T^{\text{nuc}}(z)$  for photo- and conversion electrons, respectively, can be represented by exponentials:

$$T^{\text{el}}(z) = A_1 e^{-\nu_1 z}, \quad T^{\text{nuc}}(z) = A_2 e^{-\nu_2 z}. \quad (6)$$

In order to simplify the general expressions the production probability  $W^s$  of the different types of particles is included in  $A_1$  and  $A_2$ . We also take into account the fact that the damping of the radiation field in a uniform medium is described by an exponential factor:

$$|\mathbf{E}(z)|^2 = |\mathbf{E}(0)|^2 \exp[-2\kappa \text{Im } \eta(\omega) z], \quad (7)$$

where  $\kappa = \omega/c$  and in the general case

$$\eta(\omega) = (\sin^2 \theta + \chi(\omega))^{1/2}, \quad (8)$$

where  $\theta$  is the grazing angle of incidence. Integrating Eq. (5), using Eqs. (6) and (7), we obtain

$$I(\omega) = A_1 \frac{\text{Im } \chi^{\text{el}}}{2\kappa \text{Im } \eta(\omega) + \nu_1} + A_2 \frac{\text{Im } \chi^{\text{nuc}}(\omega)}{2\kappa \text{Im } \eta(\omega) + \nu_2}. \quad (9)$$

For nongrazing propagation angles, when  $\sin^2 \theta \gg \chi(\omega)$ , the square root in Eq. (8) can be extracted approximately, and then

$$\text{Im } \eta(\omega) = \text{Im } \chi(\omega) / 2 \sin \theta. \quad (10)$$

In Mössbauer conversion spectroscopy it is usually assumed that

$$\kappa \text{Im } \eta \ll \nu_{1,2}, \quad (11)$$

and then, to within the background and normalization constants, the conversion-electron yield spectrum corresponds to the resonance absorption spectrum of the medium:

$$I(\omega) \sim \text{Im } \chi^{\text{nuc}}(\omega) + \text{const}. \quad (12)$$

We note immediately that in this case [i.e., when the condition (11) is valid] the secondary-particle yield function influences the shape of the recorded spectrum only for layered nonuniform samples. In this case

$$I^s(\omega) \sim \int_0^\infty \text{Im } \chi^{\text{nuc}}(z, \omega) T(z) dz + \text{const} \quad (13)$$

and, therefore, depth-selective investigation of the hyperfine parameters as a function of depth  $\text{Im } \chi^{\text{nuc}}(z, \omega)$  is possible, if information is available about the yield function  $T(z)$ . Conversely, the conversion-electron spectrum makes it possible to determine the yield function  $T(z)$  of the recorded electrons, if it is possible to determine independently the sequences and thicknesses of layers with different hyperfine parameters  $\text{Im } \chi^{\text{nuc}}(z, \omega)$  (for example, with the help of layer-by-layer etching or preparation of a pre-

scribed layered structure). It is obvious that at best such investigations give a quite rough approximation for the yield function.

If, however, the inequality (11) is not satisfied and the resonant dependent of the denominators in Eq. (9) becomes significant, the yield function will distort the resonant absorption spectrum when the secondary radiation is recorded. Moreover, although  $\text{Im } \chi^{el}$  (photoelectric absorption) is not a resonant function of the energy of the incident radiation, the second term in Eq. (9) nonetheless does exhibit such behavior due to the presence of the resonant denominator. Since the two terms in Eq. (9) depend differently on  $\omega$  (even if the yield functions of the photo- and conversion electrons are identical), the contribution of photoelectrons to the recorded spectrum introduces its own energy dependence. The experimentally observed asymmetry<sup>14</sup> of the background line in the secondary-electron yield spectrum is a manifestation of the existence of such a dependence.

Specifically for grazing angles of propagation the radiation is damped in the sample at depths comparable to and even less than the depths from which the secondary electrons can reach the detector, i.e., now

$$\kappa \text{Im } \eta \sim \nu_{1,2}. \quad (14)$$

In this case, even when the medium is uniform, the production probability  $P^s$  of secondary radiation is different at different depths, since the amplitude of the radiation field exciting the secondary radiation varies with depth:  $\mathbf{E} = \mathbf{E}(z)$  in Eqs. (1) and (4). In the grazing arrangement of the experiment the influence of the electron yield function is always significant.

In the case of ultrathin surface layers, however, the situation is actually much more complicated than the one considered above, because within a  $\sim 5$ – $10$  nm thick layer at the surface even quite perfect samples characteristically have significant structural distortions, anomalous density variations, oxide phases, and hyperfine parameters which are different from those in the interior. Obviously, the model of a semi-infinite uniform medium is completely unsuitable for describing the Mössbauer spectra obtained in grazing-incidence geometry.

Returning to the general expression (5) and taking into account Eqs. (1) and (4), we can see that the yield spectrum of secondary radiation in grazing-incidence geometry is determined by three functions of depth which appear in the integrand:  $\hat{\sigma}^{nul}(z, \omega)$ ,  $\mathbf{E}(z, \omega)$ , and  $T(z)$ . It is obvious that in order to find  $T(z)$  from the experimental data it is necessary to have information about the profiles of the resonance parameters of the medium  $\hat{\sigma}^{nul}(z, \omega)$ . We solved this problem by fitting the Mössbauer mirror-reflection spectra, which were measured simultaneously with the secondary-radiation yield spectrum. In addition, the change in the amplitude of the radiation field as a function of depth  $\mathbf{E}(z, \omega)$  must be calculated correctly. In the case of mirror-reflection of radiation from an anisotropic layered medium this problem requires a special analysis.

### 3. STRUCTURE OF THE RADIATION FIELD IN A LAYERED ANISOTROPIC MEDIUM UNDER TOTAL REFLECTION CONDITIONS

The theory of radiation propagation in a layered medium under conditions of total reflection is well-known from optics.<sup>16</sup> In the general case of an anisotropic layered medium the propagation matrix, which describes the simultaneous transformation of several components of the radiation field, can be used effectively in order to take into account the forward and backward propagating waves as well as the possible transformation of the polarization of the radiation. In optics the independent components are taken to be the tangential components of the electric field  $[\mathbf{qE}(z)]$  and magnetic field  $\mathbf{H}_t(z) - [\mathbf{q}(\mathbf{qE})]$  of the radiation ( $\mathbf{q}$  is a unit vector normal to the surface):

$$\frac{d}{dz} \begin{pmatrix} \mathbf{H}_t(z) \\ [\mathbf{qE}(z)] \end{pmatrix} = i\kappa \hat{M}(z) \begin{pmatrix} \mathbf{H}_t(z) \\ [\mathbf{qE}(z)] \end{pmatrix}. \quad (15)$$

When the Mössbauer radiation propagates at grazing angles and when we take into account the smallness of the susceptibility  $\hat{\chi}$  of the medium, the  $4 \times 4$  differential propagation matrix  $M(z)$  has a quite simple form:<sup>17</sup>

$$\hat{M} = \begin{pmatrix} (\mathbf{a}\hat{\chi}\mathbf{q})\mathbf{ba} & \hat{I} - \mathbf{bb}[1 - (\mathbf{a}\hat{\chi}\mathbf{a})] \\ \hat{I} - \mathbf{aa}[1 - (\mathbf{q}\hat{\chi}\mathbf{q})] & (\mathbf{q}\hat{\chi}\mathbf{a})\mathbf{ab} \end{pmatrix}, \quad (16)$$

where  $\mathbf{b}$  is the tangential component of the wave vector of the incident wave in units of  $\omega/c$ ,  $\mathbf{b} = \cos \theta$ , and  $\mathbf{a}$  is a vector perpendicular to the reflection plane:  $\mathbf{a} = [\mathbf{bq}]$ ,  $|\mathbf{a}| = |\mathbf{b}|$ , and  $\mathbf{I} = 1 - (\mathbf{qq})$ .

The integral propagation matrix  $L(d)$ , which is the solution of Eq. (15) in a film of thickness  $d$ , relates the tangential vectors  $\mathbf{H}_t$  and  $[\mathbf{qE}]$  at the upper and lower surfaces of the film. Since at the top surface of the film the radiation field is a coherent superposition of the incident and mirror-reflection waves and at the bottom surface only transmitted waves exist, it is easy to write down the general solution of the boundary-value problem as follows:

$$\hat{r} = \left[ (\hat{\gamma}^d, -\hat{I}) \hat{L}(d) \begin{pmatrix} \hat{I} \\ \hat{\gamma}^r \end{pmatrix} \right]^{-1} \left[ (-\hat{\gamma}^d, \hat{I}) \hat{L}(d) \begin{pmatrix} \hat{I} \\ \hat{\gamma}^0 \end{pmatrix} \right], \quad (17)$$

where  $\hat{r}$  is a planar tensor which relates the tangential vector  $\mathbf{H}_t^r$  of the mirror-reflected wave to the vector  $\mathbf{H}_t^0$  of the incident wave,  $\hat{\gamma}^{0,r,d}$  are the so-called impedance tensors<sup>16</sup> for the incident, specularly reflected, and transmitted waves, respectively, which transforms the tangential vector  $\mathbf{H}_t$  into  $[\mathbf{qE}]$  in each wave:

$$\mathbf{H}_t^r = \hat{r}\mathbf{H}_t^0, \quad [\mathbf{qE}^{0,r,d}] = \hat{\gamma}^{0,r,d}\mathbf{H}_t^{0,r,d}. \quad (18)$$

For the case  $\hat{\chi}(z) = \text{const}$  the solution of Eq. (15) has the form of a  $4 \times 4$  exponential matrix, and an analytic solution can be constructed using the approximations employed in Mössbauer optics.<sup>17</sup> There is a simple and efficient algorithm for computer calculations:

$$\exp\{i\kappa d \hat{M}\} = \left( \hat{E} + \frac{(i\kappa d \hat{M})}{2k} \right)^{2k}, \quad k \rightarrow \infty, \quad (19)$$

where  $\hat{E}$  is a  $4 \times 4$  unit matrix and  $k$  is chosen so as to obtain the required accuracy.

In the case of an isotropic interaction (or when the analysis can be performed separately for each characteristic polarization, if the polarizations are identical for the entire layered medium) the integral propagation matrix has the form

$$e^{ik\hat{M}d} = \begin{pmatrix} \cos Q & \frac{i}{\eta} \sin Q \\ i\eta \sin Q & \cos Q \end{pmatrix}, \quad (20)$$

where  $Q = \kappa d \eta$ , and this  $2 \times 2$  integral propagation matrix now describes the transformation of the scalar amplitude of the field and its  $z$  derivative.

In order to solve the matrix differential equation (15) in the case of a layered-nonuniform medium, the medium is usually divided into layers which are thin enough so that the parameters of the medium can be assumed to be constant in the layers. The solutions are matched automatically, since  $\mathbf{H}_i(z)$  and  $[\mathbf{qE}(z)]$  are continuous on the interfaces of the layers. In this approach the integral propagation matrix in Eq. (17) is calculated as the product of matrix exponentials of the separate layers.

The tangential amplitudes of the field can be represented in exactly the same manner as a function of the depth  $z$  in the following general form:

$$\begin{pmatrix} \mathbf{H}_i(z) \\ [\mathbf{qE}(z)] \end{pmatrix} = \exp\{ik\xi\hat{M}_n\} \cdots \exp\{ikd_1\hat{M}_1\} \begin{pmatrix} \mathbf{H}_i(0) \\ [\mathbf{qE}(0)] \end{pmatrix}, \quad (21)$$

where  $d_i$  and  $\hat{M}_i$  are the thickness and differential propagation matrix in the  $i$ th layer,  $i = 1, \dots, n$ ;  $z = d_1 + d_2 + \dots + d_{n-1} + \xi$ , where  $\xi$  is measured from the boundary of the  $n$ th layer. In order to prescribe the differential propagation matrices in each layer the susceptibility  $\hat{\chi}_n$  of the  $n$ th layer must be completely determined. The susceptibility depends on a very large number of different parameters: the electron density of the layer, the parameters of the resonance spectrum (energy, width, and amplitude of the lines and the character of the anisotropy), the density of nuclei which exhibit a given hyperfine interaction (the phase density), and so on. The calculation of  $\hat{\chi}_n$ , using the layer parameters found by analyzing the mirror-reflection spectra, is described below in Sec. 5. The total electric-field vector  $E(z)$  of the radiation is determined uniquely in terms of  $\mathbf{H}_i(z)$  and  $[\mathbf{qE}(z)]$

$$\mathbf{E}(z) = (\mathbf{qa})\mathbf{H}_i(z) + (\mathbf{ab})[\mathbf{qE}(z)]. \quad (22)$$

It is important to note that in our geometry the radiation field giving rise to the secondary radiation is different from the field of the incident wave even at the surface itself, where the field is a coherent superposition of the incident and mirror-reflection waves. Near the critical angle for total external reflection, when the incident and mirror-reflected waves add in phase, the amplitude of the field at the surface is almost doubled. For this reason, a spike is observed near the critical angle in the angular dependence of the yield of secondary radiation which emerges from a

shallow depth. The yield function or the depth of the atoms emitting the secondary radiation can be judged from the magnitude of this spike.<sup>10-12</sup> It is obvious that  $\mathbf{H}_i(0)$  and  $[\mathbf{qE}(0)]$  in Eq. (21) can be determined only after the reflection problem is solved.

The damping of the field in the layered nonuniform medium, described adequately by Eq. (21), has a non-monotonic oscillatory character: At some depths the field amplitude can exceed that at the surface. Actually, here a system of standing waves develops, whose structure influences the secondary-radiation yield just as in the case of standing x-ray waves, existing under the conditions of x-ray diffraction. We note that it is quite simple to use the unusual structure of the radiation field under the conditions of total reflection—which makes it much more complicated to interpret the secondary-radiation yield data—in other problems for analyzing the structure of films.<sup>18</sup>

#### 4. EXPERIMENT

The experiment was performed on the special SM 1101 TER spectrometer, described in detail in Ref. 19. The most important features of this apparatus are the possibility of obtaining a well-collimated beam of Mössbauer radiation, reliable alignment of the sample in a reflection position with a prescribed glancing angle  $\theta$ , and the special construction of the detector.

An important condition of experiments in grazing-influence geometry is that reasonable luminosity with collimation sufficient for observing specular reflection ( $\sim 0.5$  mrad), taking into account the extremely small dimensions of the beam interacting with the surface of the sample at grazing angles of incidence, must be preserved. We therefore tried to use the largest possible samples as well as to optimize the geometric parameters of the collimation apparatus. The collimation apparatus consisted of two slit diaphragms, whose aperture range is  $(0-1) \pm 0.02$  mm. The slits were placed at the ends of a 400–600 mm long telescopic collimation tube, and they were aligned with the help of adjusting pins.

The sample was aligned by the optical method. For this the  $\gamma$ -ray source was replaced by a light source, and an adjustment screen was positioned 1 meter from the center of the sample. The grazing angle of the incident radiation could be determined to within  $\sim \pm 0.5$  mrad according to the distance between the position of a light stripe before and after the sample is moved into the beam zone (mirror stripe). The grazing angle  $\theta$  was varied with the help of a goniometer (from an x-ray diffractometer) that varied the slope of the sample from 0 to 30 mrad.

In order to record the secondary electrons as well as the secondary x-rays the sample was inserted into one of the chambers of a two-chamber gas proportional counter. A He + 8%CH<sub>4</sub> mixture was used in this chamber in order to record the electrons and an Ar + 8%CH<sub>4</sub> mixture was used in the other chamber in order to record the x-rays. The existence of the two chambers made it possible to conduct these measurements simultaneously. The electrons were recorded with the chosen parameters of the detector without resolving the electrons in energy over the range

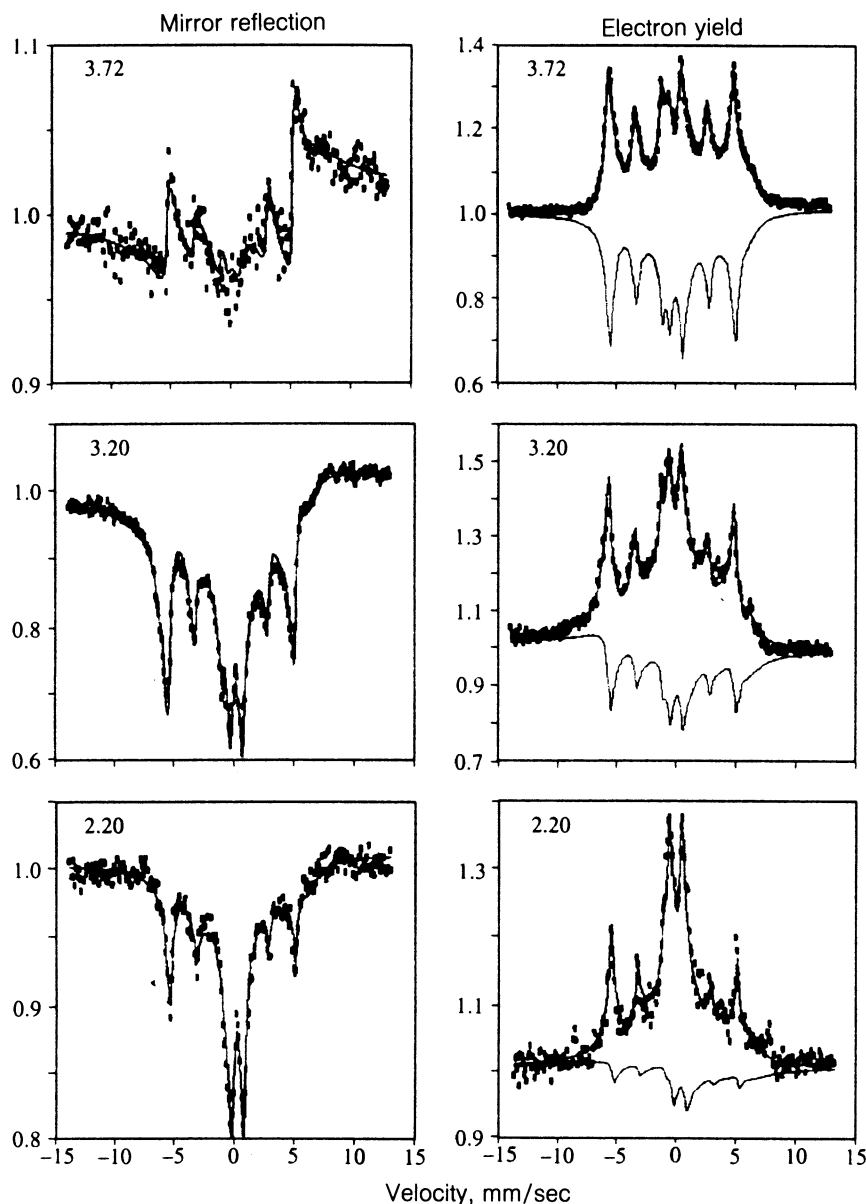


FIG. 1. Experimental Mössbauer mirror-reflection spectra (left side) and secondary-electron yield spectra (right side) for different grazing angles of the incident radiation. The angles are given in mrad. Solid lines—calculation for optimized parameters of the medium. Dashed lines in the figures on the right—photoelectron yield (background line). Here and below the spectra are normalized to the intensity of the off-resonance radiation.

1–20 keV. The efficiency of the detector for electrons in different energy groups was not investigated. In order to measure the Mössbauer conversion spectra in the normal geometry thin beryllium windows were installed at the top of the detector chambers. In addition, optically transparent organic glass windows were inserted in the body of the counter, practically in the plane of the sample, in order to allow the passage of the radiation beam at a grazing angle with respect to the surface of the sample and for recording the mirror-reflected beam.

A ribbon source ( $2 \times 8$  mm) with an activity of 20 mCi was specially prepared for the Mössbauer experiments in the grazing-incidence geometry. For the chosen divergence of the collimated radiation the collection time of each spectrum at the grazing angle was  $\sim 5$ –7 days.

The experimental sample consisted of a  $\sim 50$  nm thick, slightly oxidized  $^{57}\text{Fe}$  film ( $\sim 95\%$  enrichment) on a polished beryllium substrate 50 mm in diameter and 10 mm

thick. The beryllium substrate was chosen in order to reduce the background.

It is significant that for each grazing angle the Mössbauer mirror-reflection spectrum and the electron-yield spectrum were measured simultaneously. This eliminated the gap in the angle when switching from one recording method to another. Such “pairs” of experimental spectra, obtained for grazing angles  $\sim 2.2$  mrad (in the total-reflection region itself),  $\sim 3.2$  mrad (immediately before the critical angle), and  $\sim 3.8$  mrad (immediately beyond the critical angle), are displayed in Fig. 1.

Figure 2 displays the  $90^\circ$  electron-yield spectrum (Mössbauer spectrum of conversion electrons in the normal geometry). Comparing it to the spectra obtained in the grazing-incidence geometry immediately reveals the difference of the contributions of separate multiplets in these spectra and demonstrates qualitatively the surface sensitivity of the grazing-incidence Mössbauer spectroscopy.

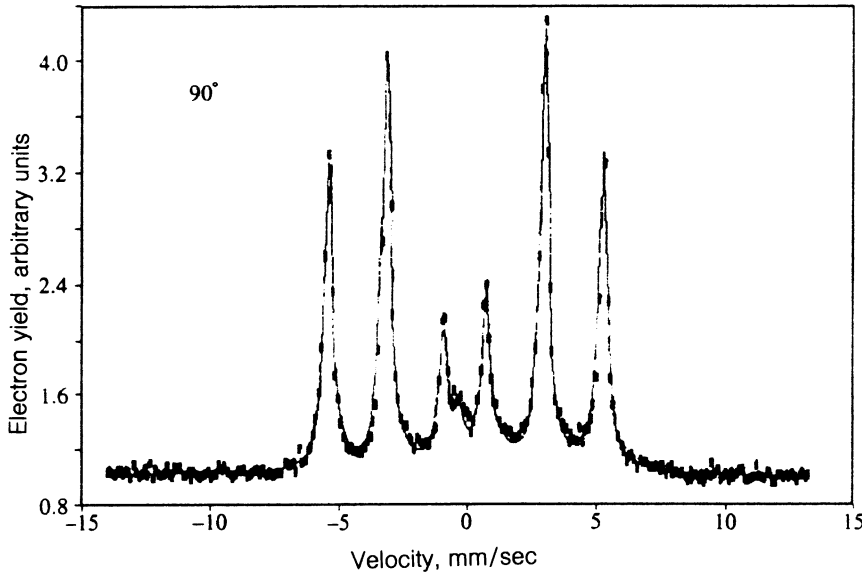


FIG. 2. Mössbauer conversion-electron spectrum measured at normal incidence of resonant radiation on the surface of the experimental sample (90° spectrum).

The transformation, observed on the left side of Fig. 1, of the shape of the lines in the experimental mirror-reflection spectra with decreasing grazing angle from essentially dispersive lineshapes to nearly absorptive lineshapes corresponds completely with the theory of mirror reflection and is a qualitative indication of the fact that the grazing angles were measured correctly.

The change in the shape of the secondary-electron yield spectrum (right half of Fig. 1) as a function of the grazing angle also cannot be missed. This pertains primarily to the background line, which is significantly asymmetric, the sign of the asymmetry changing at the transition through the critical angle. The reason for the asymmetry was explained qualitatively in Ref. 14. The quantitative analysis of these spectra undertaken in this work makes it possible to obtain unique information about the yield functions of photo- and conversion electrons in ultrathin surface layers.

## 5. INTERPRETATION OF THE EXPERIMENTAL RESULTS

The theoretical analysis of the experimental results which we undertook in order to determine the yield functions of secondary electrons was based on the following general expression describing the shape of the Mössbauer secondary-radiation yield spectra:

$$I(w_s) = \int_{-\infty}^{\infty} A(\omega_s - \omega) \times \left[ \frac{1}{2} \int_0^{\infty} [\mathbf{E}(z, \omega) * \hat{\sigma}^{\text{nucl}}(z, \omega) \mathbf{E}(z, \omega)] T^{\text{nuc}}(z) dz + \frac{\omega}{8\pi} \int_0^{\infty} \text{Im} \chi^{\text{el}}(z) |\mathbf{E}(z, \omega)|^2 T^{\text{el}}(z) dz \right] d\omega. \quad (23)$$

We did not exclude a priori the possibility that the yield functions  $T^{\text{el}}(z)$  and  $T^{\text{nuc}}(z)$  of photo- and conversion electrons, respectively, can be different. Just as in the case (6), the factors  $w_s^i$ , which are the probability of the production of secondary  $s$  radiation in a single absorption

event, are included in the yield function. As usual, the integration over  $\omega$  corresponds to the convolution of the theoretical resonance spectrum with the source lineshape  $A(\omega)$ . In our numerical calculations the integration over the depth  $z$  was replaced by summation over differential layers, whose thickness  $\Delta z = 0.2$  nm was small enough in order to take into account correctly the change in the amplitude of the field  $\mathbf{E}(z, \omega)$  with depth.

For our model analysis the experimental film was arbitrarily divided into seven layers within which the parameters  $\hat{\chi}_n^{\text{nuc}}(\omega)$ ,  $\hat{\sigma}_n^{\text{nucl}}(\omega)$ , and  $\hat{\chi}_n^{\text{el}}$  [but not the amplitude of the field  $\mathbf{E}(z, \omega)$ ] of the medium were assumed to be constants. The problem of taking into account the anisotropy of the nuclear resonance interaction was significantly simplified by making the quite obvious assumption that if the magnetic anisotropy of the film is not completely planar, it is at least axially symmetric. In this case the nuclear susceptibility tensor is replaced by a scalar, whose value is different for the two characteristic polarizations of the radiation. Thus we describe the susceptibility of each  $n$ th layer with the help of the expression

$$\chi_n = \chi_n^{\text{el}} - F \sum_k V_{n,k} \sum_i \frac{A'_{i,k} \Gamma'_{i,k} / 2}{E - E_{i,k} + i \Gamma'_{i,k} / 2}, \quad (24)$$

where  $E_{i,k}$ ,  $A'_{i,k}$ , and  $\Gamma'_{i,k}$  are the position, amplitude, and width of the  $i$ th resonance lines of the  $k$ th multiplet, and the matrix  $V_{n,k}$  determines the density of different multiplets in separate layers.

The line amplitudes and widths  $A'_{i,k}$  and  $\Gamma'_{i,k}$  in Eq. (24) characterize only a resonant sample. It is well known that the experimentally determined amplitudes  $A_{i,k}$  and widths  $\Gamma_{i,k}$  of the resonance lines also depend on the source lineshape. Under the "thin-absorber" assumption (which is practically always valid for analysis of the standard 90° conversion spectra), the following relations are evidently satisfied:

$$\Gamma'_{i,k} = \Gamma_{i,k} - \Gamma_s, \quad A'_{i,k} = A_{i,k} \frac{\Gamma_{i,k}}{\Gamma_{i,k} - \Gamma_s}. \quad (25)$$

where  $\Gamma_s$  is the source linewidth.

Taking into account the magnetic anisotropy of the film, for  $\sigma$  polarization of the magnetic field of the radiation we employed the coefficients  $A_{i,k}$  obtained by fitting the 90° electron-yield spectrum and for  $\pi$  polarization the amplitudes of the second and fifth lines were selected by an independent method.

It is convenient to normalize the line intensities in each multiplet as follows:

$$\sum_i A'_{i,k} \Gamma'_{i,k} / 2 = 1. \quad (26)$$

Then the coefficient  $F$ , determining the absolute value of the nuclear susceptibility, is found from

$$F = \frac{\pi}{\kappa^3} \frac{2I_e + 1}{2I_g + 1} N f_M Q \Gamma_{\text{nat}} \frac{1}{1 + \alpha}, \quad (27)$$

where  $f_M$  is the probability amplitude of the Mössbauer effect,  $\Gamma_{\text{nat}}$  is the natural linewidth of the Mössbauer level,  $I_{e,g}$  are the spins of the excited and ground states of the Mössbauer transition,  $Q$  is the enrichment with the Mössbauer isotope,  $N$  is the density of nuclei per unit volume, and  $\alpha$  is the internal conversion coefficient. Taking  $f_M = 0.7$ ,  $Q = 0.9$ ,  $N = 8.47 \cdot 10^{-2} \text{ \AA}^{-3}$ ,  $\lambda = 0.086 \text{ nm}$ , and  $\alpha = 9$  we obtain the following value for the coefficient  $F$ :

$$F = 8.35 \cdot 10^{-6} \text{ mm/sec.} \quad (28)$$

For this value of  $F$  and the normalization of  $A_{i,k}$  in Eq. (26) the matrix elements  $V_{n,k}$  are obviously normalized to the density of the nuclear interaction in  $\alpha$ -iron enriched up to 90% at room temperature, i.e., it is these elements that take into account all possible reasons for the fact that the nuclear susceptibility in the layer is lower than in pure  $\alpha$ -iron.

Besides the enrichment (which is known beforehand for each specific sample) these reasons are as follows: 1) the change in the density of resonant nuclei due to oxidation, roughness, etc. and 2) the change in the probability of the Mössbauer effect in the surface layers. We note that in our investigations it is very difficult to separate these two factors. For this reason in what follows we shall refer to  $V_{n,k}$  as the relative densities of resonant nuclei (though it would probably be more accurate to call them the relative densities of the nuclear resonance interaction), incorporating into this concept also the dependence of  $\chi_n^{\text{nuc}}$  on the probability of the Mössbauer effect.

According to the forgoing theoretical analysis, the problem of determining the electron yield functions is directly related to the possibility of describing accurately the change in the amplitude of the radiation field with depth. Near angles of total external reflection the radiation field in the medium (and even on the surface itself) depends directly on the change in the density and composition of the sample in each layer. Such information can be obtained by analyzing the mirror-reflection spectra at different grazing angles.

In contrast to standard Mössbauer spectroscopy, by analysis of the grazing-incidence spectra we shall mean not the decomposition of the spectrum into separate multiplets

TABLE I. Mössbauer parameters of the sample.

No.	Multiplets	%	mm/s	$\Delta E_Q$ , mm/s	$H_{\text{eff}}$ , T
1	sextet I ( $\alpha$ -Fe)	70	0.01	—	33.1
2	sextet II	16	0.54	0.14	36.4
3	sextet III	10	0.00	0.0	32.0
4	doublet $\text{Fe}^{3+}$	3	0.31	1.03	—
5	doublet $\text{Fe}^{2+}$	1	0.78	1.56	—

Note: The isomeric shift ( $\delta$ ) is given with respect to  $\alpha$ -Fe. The error in  $\delta$  and  $\Delta E_Q$  is  $\pm 0.05 \text{ mm/sec}$ .

consisting of Lorentzian lines but rather model calculations whose objective is to determine the electron-density quantities  $\text{Re } \chi_n^{el}$  and  $\text{Im } \chi_n^{el}$  and the densities of different hyperfine interactions  $V_{n,k}$  in each layer. The parameters of the multiplets, however, are determined by fitting the 90° electron-yield spectrum (see Fig. 2), and only the multiplets that are manifested too weakly in this spectrum can be refined by modeling the grazing-incidence Mössbauer spectra.

In searching for the depth profile of different hyperfine interactions, i.e., by varying the matrix elements  $V_{n,k}$ , the relative number of nuclei which exhibit this hyperfine interaction should not change. This requirement can be expressed as follows:

$$\sum_n V_{n1} d_n : \sum_n V_{n2} d_n : \sum_n V_{n3} d_n : \dots = S_1 : S_2 : S_3 : \dots, \quad (29)$$

where  $S_k$ , for  $k = 1, 2, 3, \dots$ , are the areas of the partial multiplets into which the 90° electron yield spectrum was decomposed and  $d_n$  are the thicknesses of the layers into which we arbitrarily divide our film.

In order to interpret our experimental spectra we employed the multiplets whose parameters are presented in Table I. The presence of  $\alpha$ -Fe (sextet 1) in our film is obvious, and its parameters are easily determined from the 90° electron yield spectrum. In order to describe correctly the ‘‘convex pedestal’’ in the grazing-incidence spectra we were forced to introduce into our analysis two additional sextets. The parameters of one sextet—an asymmetric strongly broadened sextet (sextet II) whose sixth line can clearly be seen in the high-velocity spectra—approximately correspond to the published data for  $\alpha$ -FeOOH.<sup>20</sup> We introduced sextet III in order to describe the distribution of the hyperfine magnetic field, which apparently occurs in  $\alpha$ -Fe (this is indicated by the asymmetry of the lines of this sextet in the 90° spectrum). The linewidths in these sextets are almost an order of magnitude greater than the linewidths in  $\alpha$ -Fe. As we have already noted, in order to refine the parameters of sextets II and III as well as of the doublets we employed the grazing-incidence spectra. The parameters of the quadrupole doublets, whose presence in the spectra indicates that our film contains iron atoms in nonmagnetic states, are typical of tri- and bivalent iron ions. The trivalent iron ions could belong to ultradispersed  $\text{Fe}_3\text{O}_4$  or  $\text{Fe}_2\text{O}_3$  inclusions in the surface layer,<sup>21</sup> and the bivalent ions could belong to inclusions of  $\text{FeOOH}$ ,  $\text{FeO}$ ,<sup>22</sup> and other compounds. It is evident that the oxidation of

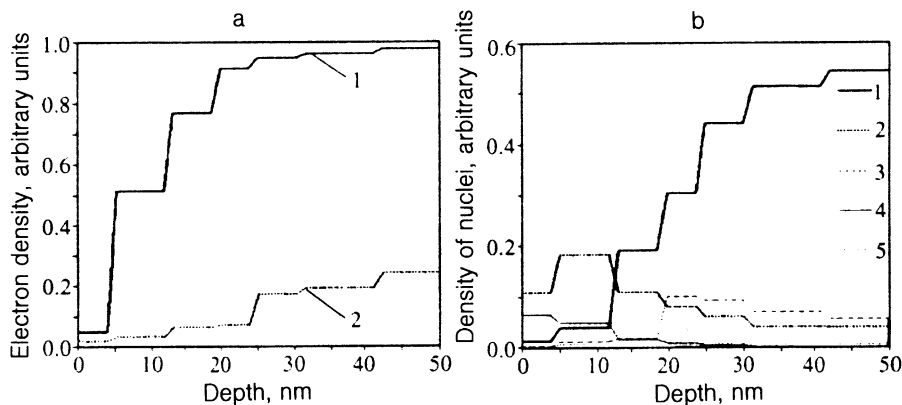


FIG. 3. a) Stepped depth profiles of the electron density (1) and photoelectric absorption (2) in units of the electron density of  $\alpha$ -Fe. b) Density of resonant nuclei exhibiting different hyperfine interactions in units of the density of resonance nuclei in enriched  $\alpha$ -Fe. The different types of hyperfine interactions are numbered according to Table I.

the ultrathin surface layer results in simultaneous coexistence of different stages of oxidation of iron.

The depth profile of the electron density and photoelectric absorption— $\text{Re } \chi^{el}$  and  $\text{Im } \chi^{el}$ —strongly influences the mirror reflection, the Mössbauer mirror-reflection spectra near the critical angle being influenced most. The stepped depth profiles obtained for our film by analyzing the spectra are displayed in Fig. 3a. The model calculations reveal that the electron-density profiles are determined much more reliably from the Mössbauer mirror-reflection spectra (owing to their unique sensitivity) than from analysis of the  $x$ -ray mirror-reflection curves.

The stepped depth profiles obtained for different multiplets by modeling the mirror-reflection spectra are displayed in Fig. 3b. The theoretical mirror-reflection spectra corresponding to these profiles of the film parameters are displayed in Fig. 1 (to the left of the solid lines). The computed spectra were angle-averaged taking into account the divergence of the incident radiation ( $\sim 0.5$  mrad); in addition, variation of the grazing angle was permitted, since the error in determining the grazing angle experimentally was also  $\sim 0.5$  mrad. The theoretical values of the grazing-incidence angle  $\theta$  which give the best agreement between theory and experiment are indicated on the spectra. As we can see, the theoretical spectra describe quite well all features of the experimental spectra. In our preceding work<sup>13,23</sup> we already demonstrated that these spectra are uniquely sensitive to variation of the profiles of different parameters, which makes our method for determining these parameters quite reliable for depths up to  $\sim 20$  nm. At greater depths the computed parameters are determined much less reliably.

The depth profiles, displayed in Figs. 3a and b, of the parameters of the medium determined by analyzing the mirror-reflection spectra are quite reasonable. It is evident that the decrease in the electron density and photoelectric absorption coefficient near the surface is due to partial oxidation of the surface layer. This is why  $\alpha$ -iron is concentrated mainly at depths exceeding 30 nm. The density of  $\text{Fe}^{3+}$  iron nuclei in the nonmagnetic state is greatest at the surface itself, and the maximum of the distribution of  $\text{Fe}^{2+}$  nuclei in the nonmagnetic state lies somewhat deeper, as expected. The magnetically ordered oxide  $\text{FeOOH}$ , described by sextet II, is found mainly at depths  $\sim 10$  nm,

and the field distribution, close in magnitude to  $\alpha$ -iron, lies in the layer preceding the almost pure  $\alpha$ -iron. It is important to note that these profiles indicate that the oxidation process has an island character, since we do not see a distinct distribution of oxidized and nonoxidized layers here: Some oxide penetrate quite deeply into the film and some  $\alpha$ -iron atoms are present in the surface layer.

After the film structure is determined, making it possible to describe correctly the radiation field in the film for different grazing angles, we can determine the yield functions: Only the unknown functions  $T^{el}(z)$  and  $T^{nuc}(z)$  remain in the integral equation (23).

As the first trial step in the modeling we employed the coefficients calculated in Ref. 6 for the case of the  $K$ -shell conversion electron yield, making the standard assumption that the photo- and conversion-electron yield functions are identical:

$$T^{el}(z) = T^{nuc}(z) = 0.74 - 2.7(z/r_B) + 2.5(z/r_B)^2, \quad (30)$$

and the electron mean free path is  $r_B = 320$  nm. However, the theoretical conversion-electron yield spectra calculated for the case (30), especially near the critical angle, were significantly different from the experimental spectra (see Fig. 4—dotted curve). Attempts to correct the situation by varying the electron mean free path  $r_B$  did not yield significant improvement. Indeed, expression (30) describes the case of the emergence of  $K$ -shell conversion electrons from a pure iron sample. It takes into account the “moderation” of this group of electrons, but it gives no idea about electron multiplication processes, which must be taken into account when the electron counter does not differentiate the electrons by energy, as corresponds to our experiment. In addition, in our case the thickness of the iron film ( $\sim 50$  nm) is significantly smaller than the electron mean-free path  $r_B = 320$  nm, and the beryllium substrate is characterized by its value of  $r_B$ . The layered nature of our sample, determined by the partial oxidation of the sample, likewise requires a separate analysis. On the basis of all these circumstances we decided not to incorporate in advance into the calculations any specific expression for the yield functions, and we decided to approximate it by a piecewise-linear function, retaining the arbitrary separation of our film into separate layers:

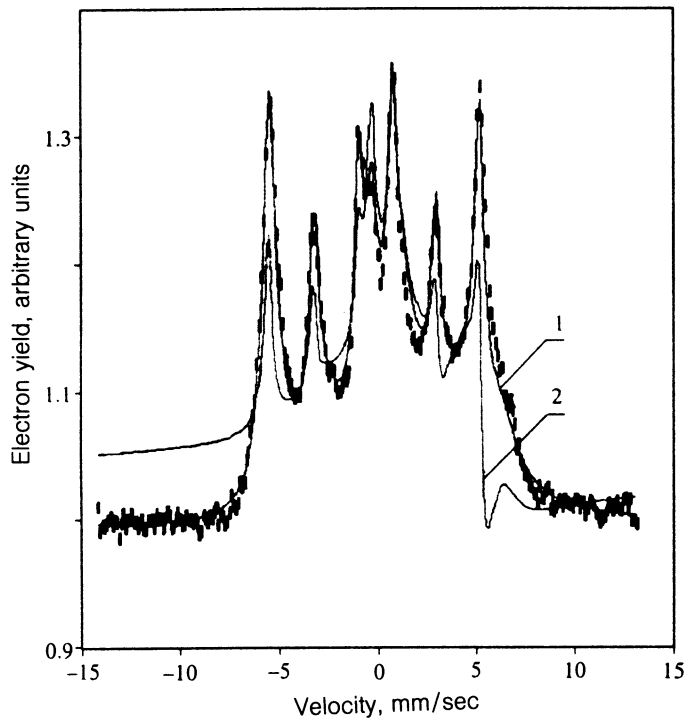


FIG. 4. Experimental and theoretical electron yield spectra for a grazing angle of 3.72 mrad. The dotted line (2) is the theoretical spectrum for the case when the photo- and conversion-electron yield function is determined by Eq. (30); the solid line (1) is the theoretical spectrum calculated using the yield functions displayed in Fig. 5.

$$\left. \begin{aligned} T^{\text{nu}}(z) &= a_{i-1} + (a_i - a_{i-1})z/d_i \\ T^{\text{el}}(z) &= b_{i-1} + (b_i - b_{i-1})z/d_i \end{aligned} \right\} 0 \leq z \leq d_i \quad (31)$$

in each layer.

In this manner we fit the coefficients  $a_i$  and  $b_i$  in the course of the model calculations of the Mössbauer electron-yield spectra at grazing incidence. The result are the functions displayed in Fig. 5. The theoretical conversion-electron yield spectra calculated for these functions are displayed in Fig. 1 (thin solid lines on the right). The agreement between theory and experiment is quite good in this case.

It is obvious the yield functions obtained differ significantly from those usually employed for interpreting the Mössbauer conversion spectra and angular dependence of photoemission under conditions of Bragg diffraction. First, the monotonic decay of these functions with depth breaks down. The maximum of these functions is shifted by  $\sim 5$

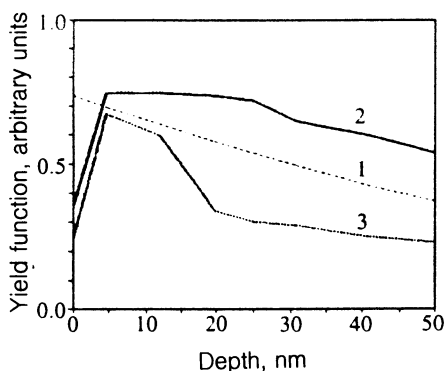


FIG. 5. Optimized photoelectron (3) and conversion electron (2) yield functions. The dashed line (1) is Liljequist's yield function (30).<sup>6</sup>

nm into the sample. Second, the photoelectron yield function is substantially different from the conversion-electron yield function.

The results are easily explained qualitatively. If the electron counter, besides the "primary" photo- and conversion electrons, records the electrons which are produced in the electron-retardation process and are obviously less energetic ("genuine secondary electrons" in the terminology of Ref. 24), then it is obvious that the maximum of the yield function will be shifted from the surface into the sample. Experiments in which the absolute yield of photoelectrons, which turned out to be significantly (tens of times) higher than predicted, was measured<sup>25</sup> support our explanation of the anomalous behavior of the yield functions. Electrons from the surface undergo virtually no collisions with other electrons and engender too few genuine secondary electrons. On the other hand, since the energies of the genuine secondary electrons are low, these electrons have virtually no influence on the photo- and conversion electron yield at great depths. The difference of the yield functions of photo- and conversion electrons is also understandable. Since the surface layer of our film contains more impurity atoms than iron atoms, the energies of both the "primary" and "secondary" photoelectrons differ significantly from the energies of the conversion electrons. Their yield functions are also correspondingly different.

We wish to emphasize that this is the first comparative determination of the photo- and conversion-electron yield functions at depths  $\sim 0-50$  nm ever made. Moreover, we are not aware of other experiments in which a similar comparative analysis could be possible. Our results undoubtedly require additional theoretical analysis.

## 6. CONCLUSIONS

In this work a completely new method of comparative determination of photo- and conversion electron yield functions was tested on a slightly oxidized nonuniform layered iron film. The method employs the appearance of resonance behavior of the photoelectron yield under the conditions of Mössbauer total reflection and includes simultaneous analysis of a series of Mössbauer mirror-reflection spectra and of the secondary-electron yield at different grazing angles.

Mathematical analysis of the spectra gave a somewhat unexpected result: The yield functions of photo- and conversion electrons recorded in our experiment without energy analysis were found to be different and, moreover, they manifested a nonmonotonic dependence on the depth in  $\sim 10$  nm layers. The observed decrease of the yield functions in an ultrathin surface layer makes it necessary to re-examine the results obtained for the thicknesses of surface layers in which anomalies are observed in the magnetic or crystalline ordering by the method of Mössbauer conversion-electron spectroscopy.

Our result can be checked in two ways.

First, our experiment should be supplemented by an analysis of the energies of the recorded electrons. This will make it possible to analyze directly the electron "multiplication" process during propagation and retardation.

Second, since the problem at hand involves a very large number of simultaneously determined parameters and employs a large volume of different experimental data, a qualitatively new mathematical approach to the solution of the problem is required. In particular, it is apparently necessary to introduce additional criteria for reliability as well as for the "error corridor" in the parameters being determined.

Third, it would be desirable to explain (or reject) this experimental result on the basis of the theory of propagation and multiplication of electrons in a nonuniform layered medium.

<sup>1</sup>M. V. Koval'chuk and V. G. Kon, *Usp. Fiz. Nauk* **149**, 69 (1986) [*Sov. Phys. Usp.* **29**, 426 (1986)].

- <sup>2</sup>V. A. Bushuev and R. N. Kuz'min, *Secondary Processes in X-Ray Optics* [in Russian], Moscow University Press, Moscow, 1990.
- <sup>3</sup>P. L. Cowan, S. Brennan, T. Jach, M. J. Bedzyk, and G. Materlik, *Phys. Rev. Lett.* **57**, 2399 (1986).
- <sup>4</sup>A. A. Novakova and R. N. Kuz'min, *Mössbauer Conversion Electron Spectroscopy and Its Applications* [in Russian] Moscow University Press, Moscow, 1989.
- <sup>5</sup>R. G. Jones and D. P. Woodruff, *Surf. Sci.* **114**, 38 (1982).
- <sup>6</sup>D. Liljequist, T. Ekdahl, and U. Baverstam, *Nucl. Instrum. Methods* **155**, 529 (1978).
- <sup>7</sup>M. V. Koval'chuk, D. Liljequist, and V. G. Kon, *Fiz. Tverd. Tela (Leningrad)* **28**, 3409 (1986) [*Sov. Phys. Solid State* **28**, 1918 (1986)].
- <sup>8</sup>E. Kh. Mukhamedzhanov, A. V. Maslov, A. N. Chuzo, and R. M. Imamov, *Poverkhnost'*, No. 3, 54 (1984).
- <sup>9</sup>M. V. Kruglov, I. K. Solomin, and A. V. Lunev, *Fiz. Tverd. Tela (Leningrad)* **28**, 322 (1986) [*Sov. Phys. Solid State* **28**, 180 (1986)].
- <sup>10</sup>B. L. Henke, *Phys. Rev. A* **36**, 94 (1972).
- <sup>11</sup>I. K. Solomin and M. V. Kruglov, *Fiz. Tverd. Tela (Leningrad)* **26**, 519 (1984) [*Sov. Phys. Solid State* **26**, 310 (1984)].
- <sup>12</sup>A. I. Chumakov and G. V. Smirnov, *Zh. Eksp. Teor. Fiz.* **89**, 1810 (1985) [*Sov. Phys. JETP* **62**, 1044 (1985)].
- <sup>13</sup>S. M. Irkaev, M. A. Andreeva, V. G. Semenov, G. N. Belozerskii, and O. G. Grishin, *Nucl. Instrum. Methods Phys. Res. B* **74**, 545 (1993) (Part I); **B 74**, 554 (1993) (Part II); Part III, in press (1994).
- <sup>14</sup>M. A. Andreeva, G. N. Belozerskii, O. V. Grishin, S. M. Irkaev, V. I. Nikolaev, and V. G. Semenov, *Pis'ma Zh. Eksp. Teor. Fiz.* **55**, 62 (1992) [*JETP Lett.* **55**, 63 (1992)].
- <sup>15</sup>M. A. Andreeva, *Zh. Tekh. Fiz.* **57**, 2009 (1987) [*Sov. Phys. Tech. Phys.* **32**, 1210 (1987)].
- <sup>16</sup>G. N. Borzdov, L. M. Barkovskii, and V. I. Lavrukovich, *Zh. Prikl. Spektrosk.* **25**, 526 (1976).
- <sup>17</sup>M. A. Andreeva and K. Rosete, *Poverkhnost'*, No. 9, 145 (1986); *Vestnik Mosk. Un-ta, Ser. 3. Fiz. Astron.* **27**, 57 (1986).
- <sup>18</sup>M. J. Bedzyk, G. M. Bommarito, and J. S. Schildkraut, *Phys. Rev. Lett.* **62**, 1376 (1989).
- <sup>19</sup>M. L. Alexandrov, G. N. Belozerskii, Yu. V. Gladkov, O. G. Grishin, S. M. Irkaev, V. I. Nikolaev, and V. G. Semenov, *Hyperfine Interactions* **71**, 1461 (1992).
- <sup>20</sup>M. Stratmann and K. Hoffmann, *Corrosion Science* **29**, 1329 (1989).
- <sup>21</sup>M. E. Brett and M. J. Graham, *J. Magn. Magn. Mater.* **60**, 175 (1986).
- <sup>22</sup>P. Ayyub, M. Multani, M. Barma, V. R. Palkar, and R. Vijayaraghavan, *J. Phys. C* **21**, 2229 (1988).
- <sup>23</sup>M. A. Andreeva, G. N. Belozerskii, S. M. Irkaev, V. G. Semenov, A. Yu. Sokolov, and N. V. Shumilova, *Phys. Status Solidi A* **127**, 455 (1991).
- <sup>24</sup>I. M. Bronshtein and B. S. Fraiman, *Secondary-Electron Emission* [in Russian], Nauka, Moscow, 1969.
- <sup>25</sup>J. S. Zabinski and B. J. Tatarchuk, *Nucl. Instrum. Methods Phys. Res. B* **42**, 379 (1989).

Translated by M. E. Alferieff